

On using intensity interferometry for feature identification and imaging of remote objects

Baris I. Erkmen*, Dmitry V. Strekalov, and Nan Yu

Jet Propulsion Laboratory, California Institute of Technology,
4800 Oak Grove Dr., Pasadena CA 91109, USA

ABSTRACT

We derive an approximation to the intensity covariance function of two scanning pinhole detectors, facing a distant source (e.g., a star) being occluded partially by an absorptive object (e.g., a planet). We focus on using this technique to identify or image an object that is in the line-of-sight between a well-characterized source and the detectors. We derive the observed perturbation to the intensity covariance map due to the object, showing that under some reasonable approximations it is proportional to the real part of the Fourier transform of the source’s photon-flux density times the Fourier transform of the object’s intensity absorption. We highlight the key parameters impacting its visibility and discuss the requirements for estimating object-related parameters, e.g., its size, velocity or shape. We consider an application of this result to determining the orbit inclination of an exoplanet orbiting a distant star. Finally, motivated by the intrinsically weak nature of the signature, we study its signal-to-noise ratio and determine the impact of system parameters.

1. INTRODUCTION

Intensity interferometry is a well-known and widely utilized technique in both classical and quantum optics, as well as in astronomy. Conventional intensity interferometry correlates the photocurrents from two pinhole detectors facing an extended thermal source, for different transverse displacements of the two detectors, obtaining an estimate of the magnitude-square of its mutual coherence function at the measurement plane. This allows one to estimate features of the source such as its diameter, or to form an image of its photon-flux density (with some regularity conditions). The earliest demonstrations of using intensity interferometry in astronomy date to Hanbury Brown and Twiss’s experiments.¹ Because intensity interferometry relies on a fourth-order field moment, the limited signature of interest has intrinsically low signal-to-noise ratio, which has limited its wide application in this field. However, with recent advances in photodetector technologies, as well as image processing techniques and capabilities, there has been a recent resurgence of interest in utilizing this technique.^{2–6}

Intensity interferometry measures the fourth-order coherence properties of the fields incident on the photodetectors, from which the coherence properties of the source can be estimated provided that the propagation through the intermediate medium is understood. In this paper, our focus is on using intensity interferometry to identify a set of features of an object—for example, its size, velocity, shape, or a fully-resolved 2D image—that is in the line-of-sight between a well-characterized source and the detectors. As such, our focus is not on the intensity covariance map *per se*, but on the perturbations to the intensity covariance map of the source alone, when an object of interest enters the path between the source and the detectors. Although we have strived to provide an exposition that is general, our specific focus in this report is a planet that is partially occluding a star.

This paper is organized as follows. In Section 2 we formulate the problem of a distant source being partially occluded by an absorptive object, using optical coherence theory and the pertinent subset of photodetection theory.⁷ Next, in Section 3 we concentrate on the intensity covariance estimate obtained by correlating the photocurrents from the two detectors, as a function of their location on the measurement plane. We show how this covariance is modified as a result of the object, and determine the key parameters that impact the signature. We introduce a differential measurement technique—i.e., taking the difference between one baseline measurement not containing the object and one with the object—that eliminates the prominent coherence signature of the source alone, so that the weak object-induced perturbation can be observed. We apply our general results to

* BIE is now at Google Inc. Send correspondence to erkmen@google.com.

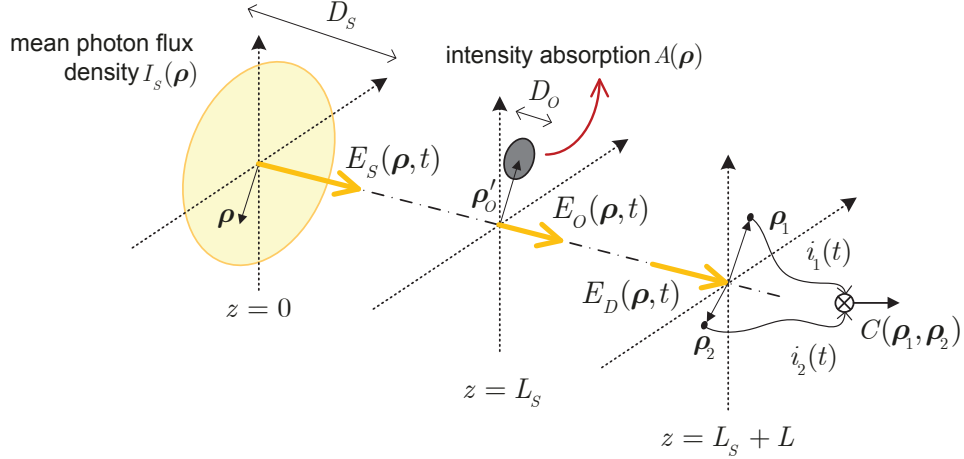


Figure 1. Block diagram of setup that measures the intensity covariance at the detector plane due to a known source and an object that is along the propagation path.

two operational scenarios: a disc-shaped source and object in (a) a typical laboratory imaging scenario, and (b) a typical stellar imaging scenario. Motivated by the intrinsically weak nature of the perturbation signal, we next focus on its signal-to-noise ratio in Section 4, highlighting various noise contributions. Finally, in Section 5 we conclude this report with some discussion of the results.

2. PROBLEM FORMULATION

Consider the scenario depicted in Fig. 1. A spatially-incoherent extended source (representing a star) is located at the $z = 0$ plane. Most natural sources emit radiation that is spatially isotropic and spectrally broadband, however, in this report our volume of interest shall be restricted to a small solid angle centered on the propagation axis z , and a small fraction of the emission spectrum centered around the wavelength λ_S . Consequently, the radiation is well modeled as a z -propagating paraxial and quasimonochromatic field arising from an extended source. We denote the scalar positive-frequency component of the source field, normalized to have units $\sqrt{\text{photons/m}^2\text{s}}$, as $E_S(\boldsymbol{\rho}, t)e^{-i\omega_S t}$, where $\omega_S \equiv 2\pi c/\lambda_S$ is the center frequency, and c is the speed of light in vacuum.

When $E_S(\boldsymbol{\rho}, t)$ corresponds to spatially-incoherent thermal radiation, it is a zero-mean Gaussian random process with a nonzero phase-insensitive correlation function^{8,9}

$$\langle E_S^*(\boldsymbol{\rho}_1, t_1)E_S(\boldsymbol{\rho}_2, t_2) \rangle = R(t_2 - t_1)I_S(\boldsymbol{\rho}_1)\lambda_S^2\delta(\boldsymbol{\rho}_2 - \boldsymbol{\rho}_1), \quad (1)$$

but no phase-sensitive correlation (i.e., $\langle E_S(\boldsymbol{\rho}_1, t_1)E_S(\boldsymbol{\rho}_2, t_2) \rangle = 0$). In Eq. (1) above, $\boldsymbol{\rho}_m$ for $m = 1, 2$ are two transverse coordinates on the $z = 0$ plane, $I_S(\boldsymbol{\rho})$ is the photon flux density in $\text{photons/m}^2\text{s}$, $R(t_2 - t_1)$ is the dimensionless temporal correlation function with $R(0) = 1$, and $\delta(\boldsymbol{\rho})$ is a two-dimensional Dirac delta function. Here, the $\lambda_S^2\delta(\boldsymbol{\rho}_2 - \boldsymbol{\rho}_1)$ term arises from our employing a delta-function approximation to the spatially-incoherent field's transverse correlation profile, which is appreciable only when $|\boldsymbol{\rho}_2 - \boldsymbol{\rho}_1|$ is on the order of a wavelength.[†]

Suppose that an opaque object (representing a planet) with finite transverse extent and negligible longitudinal extent is L_S m away from this source's transverse plane along the propagation path. We represent its photon-flux absorption density as $A(\boldsymbol{\rho} - \boldsymbol{\rho}_O)$ where $\boldsymbol{\rho}_O$ is the displacement of the center of the object on the $z = L_S$ plane.[‡]

[†]We have assumed in Eq. (1) that the correlation function is separable into the product of a function that only depends on the spatial variables, and one that only depends on the temporal variables. This separability need not hold in general—in particular, the spatial correlation could be a function of the frequency of monochromatic field components—but it is employed here as a simplification without significant loss in applicability, due to our assumption that the regime of interest is in a narrow band around ω_S .

[‡]We will carry the displacement term explicitly throughout our derivation, because it will be relevant to do so in several of the approximations we employ to arrive at our final result.

Then, the field emerging from the $z = L_S$ plane after interacting with the object is given by

$$E_O(\boldsymbol{\rho}, t) = \frac{\sqrt{1 - A(\boldsymbol{\rho} - \boldsymbol{\rho}_0)} e^{i\phi(\boldsymbol{\rho})}}{i\lambda_S L_S} \int d\boldsymbol{\rho}' E_S(\boldsymbol{\rho}', t - L_S/c) e^{ik_S L_S + ik_S |\boldsymbol{\rho} - \boldsymbol{\rho}'|^2 / (2L_S)} \quad (2)$$

where $\phi(\boldsymbol{\rho})$ is the phase profile of the object, included for completeness, but otherwise unimportant for the analysis that follows.

We assume that the observations are performed on the $z = L_S + L$ plane, wherein two pinhole photodetectors are placed at the transverse coordinates $\boldsymbol{\rho}_1$ and $\boldsymbol{\rho}_2$, respectively. The stochastic photocurrents, $i_1(t)$ and $i_2(t)$, generated by these detectors as a result of the incident field $E_D(\boldsymbol{\rho}, t)$ have the following first and second-order (conditional) moments:

$$\langle i_m(t) | E_D(\cdot) \rangle = \eta_m A_m \int d\tau |E_D(\boldsymbol{\rho}_m, \tau)|^2 h_m(t - \tau) \quad (3)$$

and for $\boldsymbol{\rho}_1 \neq \boldsymbol{\rho}_2$,

$$\langle \Delta i_m(t) \Delta i_k(u) | E_D(\cdot) \rangle = \delta_{m,k} \eta_m A_m \int d\tau |E_D(\boldsymbol{\rho}_m, \tau)|^2 h_m(t - \tau) h_m(u - \tau), \quad (4)$$

where we have normalized by the electron charge such that $i_m(t)$ for $m = 1, 2$ are in photoelectrons/s (pe/s). In these expressions, $\Delta i_m(t) \equiv i_m(t) - \langle i_m(t) | E_D(\cdot) \rangle$ are the photocurrent fluctuations around the mean, η_m are the quantum efficiencies of the two detectors, A_m are the areas of their photosensitive surface, and $h_m(t)$ are their baseband impulse responses, which includes any filtering that follows them prior to the correlation measurement. In order to eliminate a featureless background, we assume that a DC notch filter is included in $h_m(t)$, such that $\int dt h_m(t) = 0$.[§] In addition, to simplify our results we have assumed that the incident fields vary negligibly over the photosensitive area of the detectors.

The correlation between the intensity fluctuations observed by the two detectors is estimated by multiplying the two photocurrents and time-averaging the product, i.e.,

$$c(\boldsymbol{\rho}_1, \boldsymbol{\rho}_2) \equiv T^{-1} \int_{-T/2}^{T/2} dt i_1(t) i_2(t), \quad (5)$$

which is repeated at different position pairs $(\boldsymbol{\rho}_1, \boldsymbol{\rho}_2)$, $\boldsymbol{\rho}_1 \neq \boldsymbol{\rho}_2$ on the $z = L_S + L$ transverse plane. This photocurrent correlation measurement converges to its ensemble average, given by

$$C(\boldsymbol{\rho}_1, \boldsymbol{\rho}_2) = \langle c(\boldsymbol{\rho}_1, \boldsymbol{\rho}_2) \rangle = \eta_1 \eta_2 A_1 A_2 \int d\tau_1 \int d\tau_2 \langle |E_D(\boldsymbol{\rho}_1, \tau_1)|^2 |E_D(\boldsymbol{\rho}_2, \tau_2)|^2 \rangle h_1(t - \tau_1) h_2(t - \tau_2) \quad (6)$$

$$= \eta_1 \eta_2 A_1 A_2 \int d\tau_1 \int d\tau_2 \langle E_D^*(\boldsymbol{\rho}_1, \tau_1) E_D(\boldsymbol{\rho}_2, \tau_2) \rangle^2 h_1(t - \tau_1) h_2(t - \tau_2) \quad (7)$$

for $\boldsymbol{\rho}_1 \neq \boldsymbol{\rho}_2$. The second line follows from the Gaussian moment factoring of the fourth-order moment of $E_D(\boldsymbol{\rho}, t)$,[§] combined with the fact that we have assumed that $h_m(t)$ blocks DC. Thus, the correlation signature of interest depends on the phase-insensitive correlation function of the detected field $E_D(\boldsymbol{\rho}, t)$.

In the upcoming sections we shall find that the image signature of the object is weak and embedded in a strong baseline signature generated by the source. Thus, we will also consider the signature obtained by differencing a scan obtained *with* the object present and one that is obtained *without* the object present. We formally express this measurement as $c_1(\boldsymbol{\rho}_1, \boldsymbol{\rho}_2) - c_0(\boldsymbol{\rho}_1, \boldsymbol{\rho}_2)$, where c_1 is the Eq. (5) measurement with the object and c_0 is the same measurement without the object. We denote its mean value as

$$\Delta C(\boldsymbol{\rho}_1, \boldsymbol{\rho}_2) \equiv \langle c_1(\boldsymbol{\rho}_1, \boldsymbol{\rho}_2) - c_0(\boldsymbol{\rho}_1, \boldsymbol{\rho}_2) \rangle, \quad (8)$$

[§]This DC photocurrent component provides information regarding the total photon flux blocked by the object, which is at the heart of the detection methodology used in the on-going Kepler mission.¹⁰ Kepler tracks slow intensity variations in a bright object, e.g., a star, to detect Earth-sized exoplanets orbiting the star and to estimate their orbital characteristics. Here we focus our analysis on the *additional* information garnered via the utilization of intensity correlations, but this does not preclude one from also using the mean photon flux registered by each detector.

which can also be expressed in terms of the difference of E_D 's magnitude-squared phase-insensitive correlation function in the two cases, namely, by replacing $|\langle E_D^*(\boldsymbol{\rho}_1, \tau_1)E_D(\boldsymbol{\rho}_2, \tau_2)\rangle|^2$ in the integrand of Eq. (7) with $|\langle E_{D,1}^*(\boldsymbol{\rho}_1, \tau_1)E_{D,1}(\boldsymbol{\rho}_2, \tau_2)\rangle|^2 - |\langle E_{D,0}^*(\boldsymbol{\rho}_1, \tau_1)E_{D,0}(\boldsymbol{\rho}_2, \tau_2)\rangle|^2$. Here $E_{D,m}$ for $m = 0, 1$ refers to the incident field when the measurement is c_m .

2.1 Phase-insensitive coherence propagation

In order to derive the phase-insensitive correlation function of $E_D(\boldsymbol{\rho}, t)$, we first return to Eq. (2), and write

$$\langle E_O^*(\boldsymbol{\rho}_1, t_1)E_O(\boldsymbol{\rho}_2, t_2)\rangle \approx [1 - A(\boldsymbol{\rho}_s - \boldsymbol{\rho}_O)] e^{ik_S\boldsymbol{\rho}_s\cdot\boldsymbol{\rho}_d/L_S} K_O^{(n)}(\boldsymbol{\rho}_d; L_S)R(t_d), \quad (9)$$

where $\boldsymbol{\rho}_s \equiv (\boldsymbol{\rho}_1 + \boldsymbol{\rho}_2)/2$, $\boldsymbol{\rho}_d \equiv \boldsymbol{\rho}_2 - \boldsymbol{\rho}_1$, $t_d \equiv t_2 - t_1$, and

$$K_O^{(n)}(\boldsymbol{\rho}; L) \equiv \frac{1}{L^2} \int d\boldsymbol{\rho}' I_S(\boldsymbol{\rho}')^{-ik_S\boldsymbol{\rho}\cdot\boldsymbol{\rho}'/L}. \quad (10)$$

The Fourier transform relation between I_S and $K_O^{(n)}$ implies that the latter's width is $\sim \lambda_S L_S/D_S$, where D_S is defined as the diameter over which the star photon-flux density $I_S(\boldsymbol{\rho})$ is appreciably greater than zero. Therefore, the validity of the approximation in Eq. (9) rests on the $\phi(\cdot)$ and $A(\cdot)$ terms having negligible variation for $(\boldsymbol{\rho}_1, \boldsymbol{\rho}_2)$ pairs that satisfy $|\boldsymbol{\rho}_d| < \lambda_S L_S/D_S$, such that they can be approximated by their value at $\boldsymbol{\rho}_s$.⁸ This approximation notably simplifies our results for propagating the object-plane coherence to the detector plane, located at $z = L + L_S$, as we shall see shortly. Similar to Eq. (2) above, the detection-plane field is given by

$$E_D(\boldsymbol{\rho}, t) = \frac{1}{i\lambda_S L} \int d\boldsymbol{\rho}' E_O(\boldsymbol{\rho}', t - L/c) e^{ik_S L + ik_S |\boldsymbol{\rho} - \boldsymbol{\rho}'|^2 / (2L)}. \quad (11)$$

Consequently, using Eq. (9), its phase-insensitive correlation function is

$$\langle E_D^*(\boldsymbol{\rho}_1, t_1)E_D(\boldsymbol{\rho}_2, t_2)\rangle = R(t_d) \left[e^{ik_S\boldsymbol{\rho}_s\cdot\boldsymbol{\rho}_d/(L+L_S)} K_O^{(n)}(\boldsymbol{\rho}_d; L + L_S) - K_D^{(n)}(\boldsymbol{\rho}_s, \boldsymbol{\rho}_d) \right] \quad (12)$$

where the first term is the source's correlation signature in the absence of any object (i.e., vacuum propagation for $L + L_S$), and

$$K_D^{(n)}(\boldsymbol{\rho}_s, \boldsymbol{\rho}_d) \equiv \frac{e^{ik_S\boldsymbol{\rho}_s\cdot\boldsymbol{\rho}_d/L - ik_S\boldsymbol{\rho}_d\cdot\boldsymbol{\rho}_O/L}}{\lambda_S^2 L^2} \times \int d\boldsymbol{\rho}'_s \int d\boldsymbol{\rho}'_d A(\boldsymbol{\rho}'_s) K_O^{(n)}(\boldsymbol{\rho}'_d; L_S) e^{ik_S\boldsymbol{\rho}_O\cdot\boldsymbol{\rho}'_d/L_e} e^{ik_S\boldsymbol{\rho}'_s\cdot\boldsymbol{\rho}'_d/L_e} e^{-ik_S\boldsymbol{\rho}_s\cdot\boldsymbol{\rho}'_d/L} e^{-ik_S\boldsymbol{\rho}_d\cdot\boldsymbol{\rho}'_s/L} \quad (13)$$

is the modification resulting from the the object of interest. Here $L_e^{-1} \equiv L_S^{-1} + L^{-1}$. In evaluating the Eq. (13) integral we make our second critical approximation. For most objects of interest in this report we have that

$$\frac{D_O}{D_S} \left(1 + \frac{L_S}{L} \right) \ll 1, \quad (14)$$

where D_O is the diameter over which the *centered* object's absorption profile $A(\boldsymbol{\rho})$ is appreciable. When this condition holds we can neglect the second phase term in the integrand of Eq. (13), thereby decoupling the integrals over $\boldsymbol{\rho}'_s$ and $\boldsymbol{\rho}'_d$. Hence, in scenarios wherein Eq. (14) holds we find that

$$K_D^{(n)}(\boldsymbol{\rho}_s, \boldsymbol{\rho}_d) \approx \frac{e^{ik_S\boldsymbol{\rho}_s\cdot\boldsymbol{\rho}_d/L - ik_S\boldsymbol{\rho}_O\cdot\boldsymbol{\rho}_d/L}}{L^2} I_S \left(-\frac{L_S}{L}\boldsymbol{\rho}_s + \frac{L_S}{L_e}\boldsymbol{\rho}_O \right) \mathcal{A} \left(\frac{k_S}{L}\boldsymbol{\rho}_d \right), \quad (15)$$

where

$$\mathcal{A}(\mathbf{k}) \equiv \int d\boldsymbol{\rho} A(\boldsymbol{\rho}) e^{-i\mathbf{k}\cdot\boldsymbol{\rho}}. \quad (16)$$

Substituting Eq. (15) into Eq. (12), and substituting that into Eq. (7), yields the photocurrent correlation

$$C(\boldsymbol{\rho}_s, \boldsymbol{\rho}_d) \approx C \frac{I_S^2(\mathbf{0})}{L^4 \beta^4} \left| \mathcal{T}_S \left(\frac{k_S \boldsymbol{\rho}_d}{L\beta} \right) - \beta^2 e^{i\frac{L_S k_S}{L^2 \beta} \boldsymbol{\rho}_s \cdot \boldsymbol{\rho}_d} \mathcal{T}_S \left(-\frac{L_S}{L}\boldsymbol{\rho}_s + \beta \boldsymbol{\rho}_O \right) \mathcal{A} \left(\frac{k_S}{L}\boldsymbol{\rho}_d \right) e^{-i\frac{k_S}{L}\boldsymbol{\rho}_d \cdot \boldsymbol{\rho}_O} \right|^2 \quad (17)$$

where $\beta \equiv 1 + L_S/L$, $\mathcal{T}_S(\boldsymbol{\rho}) \equiv I_S(\boldsymbol{\rho})/I_S(\mathbf{0})$, $\mathcal{T}_S(\mathbf{k}) \equiv \int d\boldsymbol{\rho} \mathcal{T}_S(\boldsymbol{\rho}) e^{-i\mathbf{k}\cdot\boldsymbol{\rho}}$, and $C \equiv \eta_1 \eta_2 A_1 A_2 [|R(t)|^2 \star h_1 \star \overleftarrow{h_2}](t)$. In the last expression we have used \star to denote convolution and $\overleftarrow{h_2}$ to denote time reversal.

Variable	Lab demo	Stellar imaging
λ_S [m]	1×10^{-6}	1×10^{-6}
L_S [m]	0.5	1.496×10^{11} (1 a.u.)
L [m]	0.5	8.948×10^{18} (290 pc)
r_S [m]	0.01	6.955×10^8
r_O [m]	0.001	6.371×10^6
β	2	$1 + 1.67 \times 10^{-8}$
γ	0.1	9.16×10^{-3}
$\lambda_S L / (2r_S)$ [m]	2.5×10^{-5}	6.433×10^3

Table 1. Two sets of parameters that will be used throughout our paper. The second column denotes a representative set of parameters that could be demonstrated in a laboratory setting. The third column denotes a parameter set consistent with imaging an exoplanet.

3. IMAGE SIGNATURES OF SCANS

To derive further insight into the image signature, let us consider the case when $\boldsymbol{\rho}_s = 0$, i.e., the two detectors are always symmetrically opposite about the optical axis. In this case, Eq. (17) simplifies to

$$C(\boldsymbol{\rho}_d) \approx \mathcal{C} \frac{I_S^2(\mathbf{0})}{L^4 \beta^4} \left| \mathcal{T}_S \left(\frac{k_S \boldsymbol{\rho}_d}{L \beta} \right) - \beta^2 T_S(\beta \boldsymbol{\rho}_O) \mathcal{A} \left(\frac{k_S}{L} \boldsymbol{\rho}_d \right) e^{-i \frac{k_S}{L} \boldsymbol{\rho}_d \cdot \boldsymbol{\rho}_O} \right|^2 \quad (18)$$

where we have dropped $\boldsymbol{\rho}_s$ from the left-hand side to simplify the notation. Recall that the first term inside the square-magnitude expression is due to the source alone, thus, the second term is the object-induced modification to the correlation signature that we seek to identify.

In the following we will consider disc-shaped objects as an analytically-tractable example and derive the resultant image signature. Suppose,

$$T_S(\boldsymbol{\rho}) = \text{circ}(|\boldsymbol{\rho}|/r_S) \equiv \begin{cases} 1 & \text{for } |\boldsymbol{\rho}| \leq r_S \\ 0 & \text{otherwise,} \end{cases} \quad (19)$$

and

$$A(\boldsymbol{\rho}) = \begin{cases} 1 & \text{for } |\boldsymbol{\rho}| \leq r_O \\ 0 & \text{otherwise,} \end{cases} \quad (20)$$

where $r_O \ll r_S$. Substituting these into Eq. (18), we can write our observed signature in terms of normalized parameters as

$$C(x, \theta) = \frac{\mathcal{C} P^2}{L^4 \beta^4} \left| \frac{2J_1(\pi x / \beta)}{\pi x / \beta} - \beta^2 \gamma^2 \text{circ}(\beta x_O) \frac{2J_1(\pi \gamma x)}{\pi \gamma x} e^{-i \pi x x_O \cos(\theta)} \right|^2, \quad (21)$$

where we have $x \equiv 2|\boldsymbol{\rho}_d|/r_S/(\lambda_S L)$ as the normalized displacement of the detectors, $x_O \equiv |\boldsymbol{\rho}_O|/r_S$ as the fractional displacement of the object relative to the source radius, $\theta \equiv \angle \boldsymbol{\rho}_d - \angle \boldsymbol{\rho}_O$ as the angular separation between the vector that connects the two detectors and the object displacement vector, $P \equiv I_S(\mathbf{0}) \pi r_S^2$ as the mean photon flux of the source, and $\gamma \equiv r_O/r_S$ as the object-to-source diameter ratio.

The mean signature in Eq. (21) indicates that the modification to the coherence measurements due to the object is proportional to γ^2 and therefore it constitutes a rather *weak* signature. Thus, we also consider the image signature from the *difference* measurement introduced in Eq. (8), wherein a scan with the object present and one without is differenced to detect the perturbation due to the object (assuming everything else remains stationary). Employing Eq. (18) we find that Eq. (8) can be expressed as

$$\Delta C(x, \theta) = \frac{\mathcal{C} P^2}{L^4 \beta^2} \gamma^2 \text{circ}(\beta x_O) \frac{2J_1(\pi \gamma x)}{\pi \gamma x} \left[-2 \frac{2J_1(\pi x / \beta)}{\pi x / \beta} \cos(\pi x x_O \cos(\theta)) + \gamma^2 \beta^2 \frac{2J_1(\pi \gamma x)}{\pi \gamma x} \right], \quad (22)$$

where we have used the normalized variables introduced earlier.

In stellar interferometry it is typically the case that $L_S \ll L$, hence, $\beta \approx 1$. In addition, we have that $\gamma \ll 1$. Thus, we can further simplify Eq. (21) to

$$C(x, \theta) \approx \frac{CP^2}{L^4} \left[\left(\frac{2J_1(\pi x)}{\pi x} \right)^2 - 2\gamma^2 \text{circ}(x_O) \frac{2J_1(\pi x)}{\pi x} \frac{2J_1(\pi \gamma x)}{\pi \gamma x} \cos(\pi x x_O \cos(\theta)) \right], \quad (23)$$

in which we have dropped the weak term proportional to γ^4 . With the same set of assumptions, the differential measurement signature from Eq. (22) simplifies to

$$\Delta C(x, \theta) \approx -2 \frac{CP^2}{L^4} \gamma^2 \text{circ}(x_O) \frac{2J_1(\pi x)}{\pi x} \frac{2J_1(\pi \gamma x)}{\pi \gamma x} \cos(\pi x x_O \cos(\theta)). \quad (24)$$

We summarize a set of typical parameter values in Table 1 for two scenarios. A feasible set of parameters for a table-top laboratory demonstration of the concept (see the column labeled *lab demo*), and a set of parameters that correspond to a Sun-size source being occluded by an Earth-size planet, and being observed from a distance equivalent to that of Kepler 20f (see the column labeled *stellar imaging*).¹⁰ In Fig. 2 we show the results pertaining to the $C(x, \theta)$ and $\Delta C(x, \theta)$ measurements for the laboratory demonstration case, and in Fig. 3 we show the same results for the stellar imaging case. In particular, subfigure (a) in both figures corresponds to $C(x, \theta)$ plotted as a function of x for different θ , whereas subfigure (b) plots the same for ΔC . Subfigure (c) corresponds to the fractional variation of the *half-width half-maximum* (HWHM) of $C(x, \theta)$ —when viewed as function of x at different θ values—as a function of the object displacement x_O . Finally subfigure (d) is the same for $\Delta C(x, \theta)$.[¶] Qualitatively, we immediately observe that the variation between different curves (corresponding to different θ values) is much more prominent for ΔC . This is an expected result, because as we have derived above, the object-dependent signature is notably weaker than the signature from the source alone, and subtracting out this dominant term highlights the variations caused by the planet.^{||} This observation is reinforced by the half-width-half-maximum estimates of the covariance functions. It is clear that the variation of this width is much more significant in the differential-measurement case.

The weakness of the object-induced signature becomes apparent in the Fig. 3 results, which show the same results as before, but for the parameters in the second column of Table 1. Now, in Fig. 3(a) the covariance functions are practically indistinguishable, which is also seen in Fig. 3(c) as a very minor variation in the HWHM as a function of x_O . All hope is not lost, however, as the differential measurement still has appreciable distinguishability in the HWHM as a function of θ as well as x_O .

4. SIGNAL-TO-NOISE RATIO

We concluded in Section 3 that, under nominal conditions applicable to a small object obscuring an extended source ($\gamma \ll 1$), the perturbation signature due to the object is weak relative to the baseline signature from the source alone. While a differential measurement can eliminate the source's baseline and improve the visibility of the object's perturbation, it will not eliminate the noise contributed by the source. In this section we derive the signal-to-noise ratio (SNR) of the differential measurement in order to develop a better appreciation for the sensitivity of this measurement.

Recall from Section 2 that the differential measurement can be expressed as $c_1(\boldsymbol{\rho}_1, \boldsymbol{\rho}_2) - c_0(\boldsymbol{\rho}_1, \boldsymbol{\rho}_2)$, where c_1 is the Eq. (5) measurement *with* the object of interest present, and c_0 is the same measurement *without* the object present. As typically these two measurements are separated by a duration significantly longer than the coherence time of the photocurrent fluctuations, it can be assumed with practically no loss of generality that the two measurements are statistically uncorrelated. Thus, the variance of the measurement is,

$$\text{Var}(c_1 - c_0) = \text{Var}(c_1) + \text{Var}(c_0) \approx 2\text{Var}(c_0) \quad (25)$$

[¶]In particular, we plot the ratio of the change in the HWHM of $C(x, \theta)$ and $\Delta C(x, \theta)$ and their respective HWHMs at $x_O = 0$.

^{||}While this subtraction will improve the visibility of the measurement signature, it will *not* change its signal-to-noise ratio.

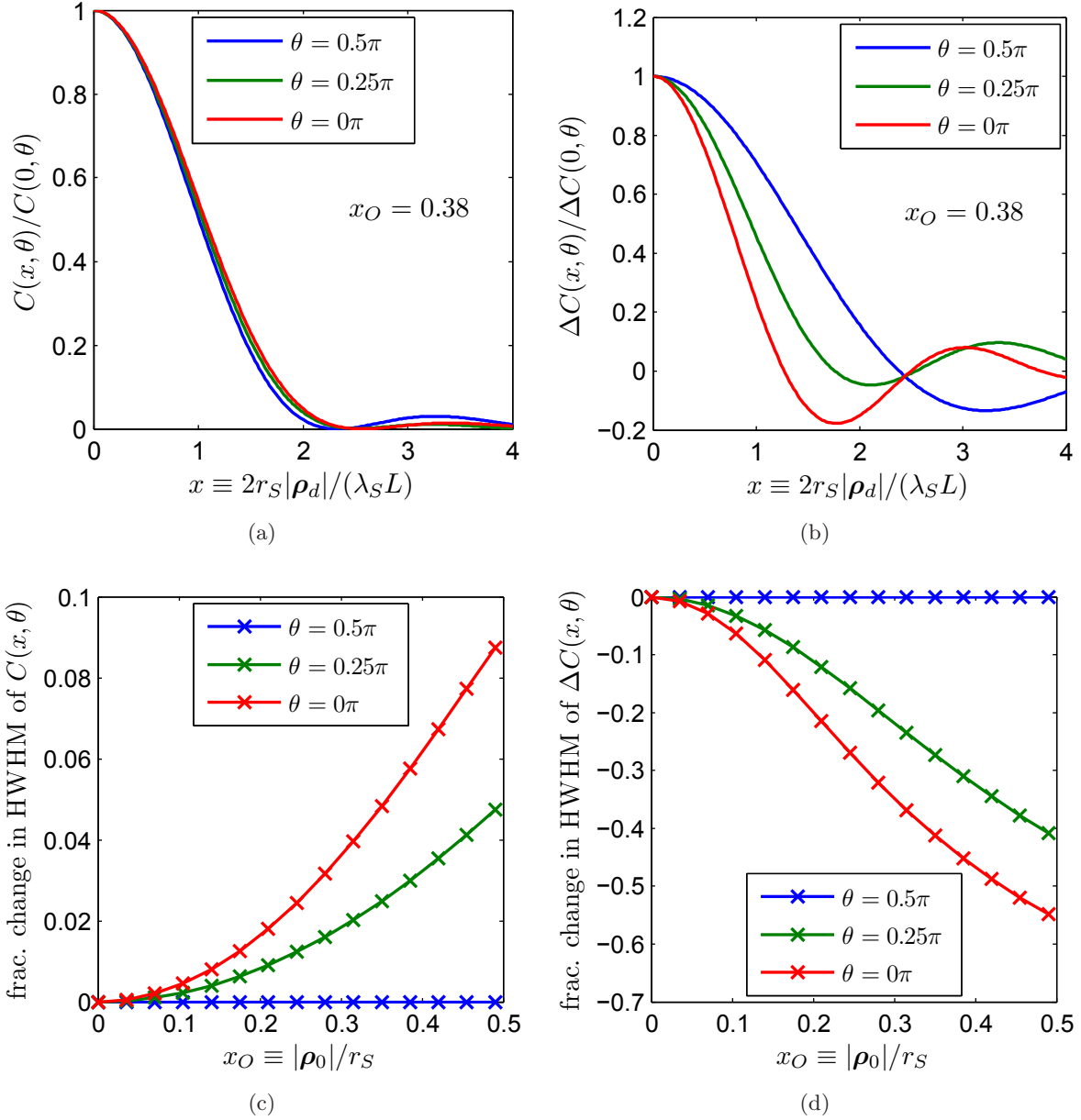


Figure 2. Image signature plots, explained in Section 3. The plots use the set corresponding to lab parameters, listed in Table 1.

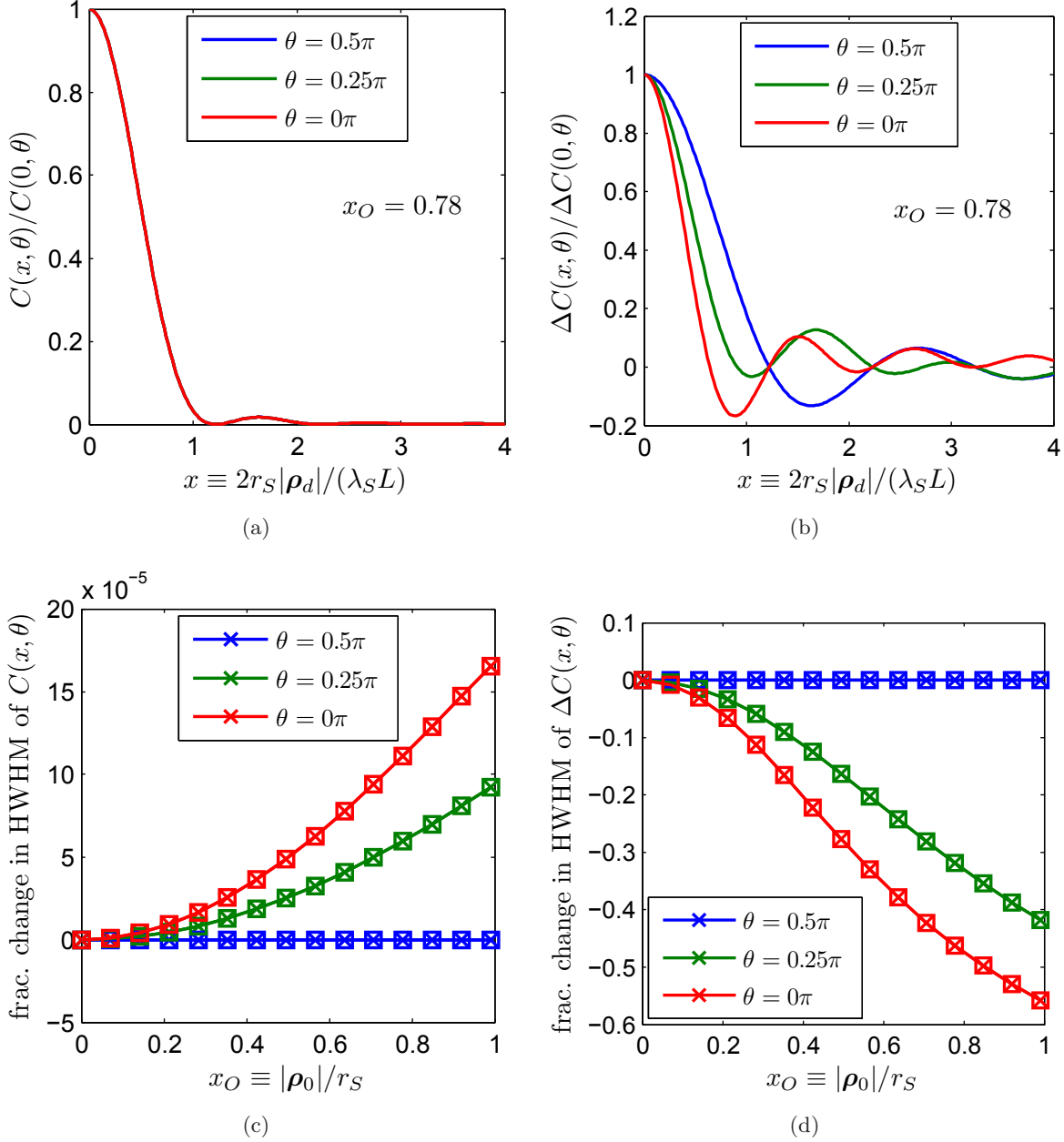


Figure 3. Image signature plots, explained in Section 3. The plots use the set corresponding to stellar parameters, listed in Table 1. In (c) and (d), the squares denote the results obtained with the approximate analytic expressions, which show excellent agreement with the results obtained from exact expressions (shown as crosses).

where the last approximation stems from our earlier observation that the object's perturbation signature is significantly weaker than that of the source when $\gamma \ll 1$. Consequently, in this regime it can be assumed that the variance of either measurement will be dominated by the source-induced shot- and excess-noise fluctuations.

The SNR can, therefore, be expressed as

$$\text{SNR} = \frac{|c_1 - c_0|^2}{\text{Var}(c_1 - c_0)} \approx \frac{|\Delta C|^2}{2\text{Var}(c_0)}. \quad (26)$$

We have derived the numerator of this expression in Section 3, thus here we concentrate on the denominator. Using the photocurrent moments given in Eqs. (3) and (4), as well as iterated expectations, it is straightforward—albeit somewhat tedious—to show that the variance can be expressed as

$$\text{Var}(c_0) = \int d\tau_1 \int d\tau_2 \int dv_1 \int dv_2 K_h(\tau_1, \tau_2) K_h(v_1, v_2) K_i(\tau_1, \tau_2, v_1, v_2), \quad (27)$$

where

$$K_h(\tau_1, \tau_2) = T^{-1} \int dt h_1(t - \tau_1) h_2(t - \tau_2), \quad (28)$$

and

$$\begin{aligned} K_i(\tau_1, \tau_2, v_1, v_2) = & \eta_1 A_1 \eta_2 A_2 \left[\langle |E_1(\tau_1)|^2 |E_2(\tau_2)|^2 \rangle \delta(\tau_1 - v_1) \delta(\tau_2 - v_2) \right. \\ & + \eta_1 A_1 \langle |E_1(\tau_1)|^2 |E_1(v_1)|^2 |E_2(\tau_2)|^2 \rangle \delta(\tau_2 - v_2) + \eta_2 A_2 \langle |E_1(\tau_1)|^2 |E_2(\tau_2)|^2 |E_2(v_2)|^2 \rangle \delta(\tau_1 - v_1) \\ & \left. + \eta_1 A_1 \eta_2 A_2 \left\{ \langle |E_1(\tau_1)|^2 |E_1(v_1)|^2 |E_2(\tau_2)|^2 |E_2(v_2)|^2 \rangle - \langle |E_1(\tau_1)|^2 |E_2(\tau_2)|^2 \rangle \langle |E_1(v_1)|^2 |E_2(v_2)|^2 \rangle \right\} \right]. \quad (29) \end{aligned}$$

Here, we have used the short-hand notation $E_m(\tau) \equiv E_D(\boldsymbol{\rho}_m, \tau)$ for $m = 1, 2$, and all ensemble averages are over the detected field $E_D(\boldsymbol{\rho}, t)$. The terms in Eq. (29) have intuitive physical origins: the first term is the covariance of common-mode fluctuations in the shot-noise (i.e., the conditional variance) from the two detectors, the term on the third line is the covariance between the signal fluctuations (i.e., the conditional mean-square) from the two detectors, and the two terms on the second line are the covariances between the shot-noise fluctuations in one detector and the signal fluctuations in the other detector.

In order to evaluate Eq. (27), we first perform Gaussian moment factoring⁸ on each term in Eq. (29). This yields expressions for every term in Eq. (29) in terms of $K_D^{(n)}(\boldsymbol{\rho}_1, \boldsymbol{\rho}_2)$, which is given in Eq. (15). Next, we assume that the AC-coupled photodetector impulse responses $h_1(t)$ and $h_2(t)$ are identical and Gaussian-shaped with e^{-2} -bandwidth Ω_B , namely,

$$h_m(t) = \sqrt{\frac{\pi\Omega_B^2}{2}} e^{-t^2\Omega_B^2/8} - \sqrt{\frac{\pi\Omega_N^2}{2}} e^{-t^2\Omega_N^2/8}. \quad (30)$$

The second term represents the DC notch with bandwidth Ω_N . Henceforth, we assume that $\Omega_B \gg \Omega_N$, which allows to us to effectively neglect the notch's contribution to any nonzero-frequency terms. Our final assumption in evaluating the Eq. (27) is that $T\Omega_B \gg 1$ and $T/T_D \gg 1$, such that we may approximate Eq. (28) as

$$K_h(\tau_1, \tau_2) = T^{-1} \text{rect} \left(\frac{|\tau_1 + \tau_2|}{T} \right) [h_1 \star \overleftarrow{h_2}](\tau_2 - \tau_1), \quad (31)$$

where \star denotes convolution and $\overleftarrow{h_2}$ denotes time reversal, as before.

For brevity, we shall opt to be content with skipping the steps of evaluating each term in the variance expression that results from following through the aforementioned steps, and state that the resultant SNR expression is given by

$$\text{SNR} = \frac{\cos^2(\theta_d)\alpha}{\sigma_{ss}^2 + \sigma_{se}^2 + \sigma_{ee}^2}, \quad (32)$$

where we have defined the terms in this expression as follows. In the most general case

$$\theta_d \equiv \angle \left\{ e^{-ik_s \boldsymbol{\rho}_s \cdot \boldsymbol{\rho}_d / (L+L_S)} [K_O^{(n)}(\boldsymbol{\rho}_d; L+L_S)]^* K_D^{(n)}(\boldsymbol{\rho}_s, \boldsymbol{\rho}_d) \right\} \quad (33)$$

which simplifies to

$$\theta_d = \pi x x_O \cos(\theta) \quad (34)$$

when the scenario is specialized to that discussed in Section 3. The numerator also includes

$$\alpha \equiv \left| \frac{K_D^{(n)}(\boldsymbol{\rho}_s, \boldsymbol{\rho}_d)}{K_O(\mathbf{0}; L + L_S)} \right|^2 = \beta^4 \gamma^4 \text{circ}(\beta x_O) \left(\frac{2J_1(\pi \gamma x)}{\pi \gamma x} \right)^2, \quad (35)$$

which, when $\gamma x \ll 1$, $\beta \approx 1$, and $\beta x_O < 1$ (as in the stellar imaging case), simplifies to $\alpha \approx \gamma^4$. The three terms in the denominator of the SNR expression are given by

$$\sigma_{ss}^2 \equiv \frac{\sqrt{2}}{\sqrt{\pi} T \Omega_B \Gamma N^2} \left[1 + \frac{T_0 \Omega_B \Gamma}{\sqrt{8} \sqrt{1 + \frac{\Omega_B^2 T_0^2}{8}}} \right], \quad (36)$$

$$\sigma_{se}^2 \equiv \frac{2\sqrt{2}}{T \Omega_B \Gamma N} \frac{1 + \frac{T_0^2 \Omega_B^2}{16}}{\sqrt{1 + \frac{T_0^2 \Omega_B^2}{32}}} \left[1 + \frac{\sqrt{2} T_0 \Omega_B \Gamma}{\sqrt{3}} \frac{\sqrt{1 + \frac{T_0^2 \Omega_B^2}{32}}}{\sqrt{1 + \frac{T_0^2 \Omega_B^2}{8}} \sqrt{1 + \frac{T_0^2 \Omega_B^2}{24}}} \right], \quad (37)$$

$$\sigma_{ee}^2 \equiv \frac{\sqrt{2\pi}}{T \Omega_B \Gamma} \sqrt{1 + \frac{T_0^2 \Omega_B^2}{16}} \left[1 + \Gamma^2 + \frac{T_0 \Omega_B \Gamma}{\sqrt{1 + \frac{\Omega_B^2 T_0^2}{8}}} \left(1 + \Gamma + \frac{\sqrt{1 + \frac{T_0^2 \Omega_B^2}{16}}}{\sqrt{1 + \frac{T_0^2 \Omega_B^2}{8}}} \right) \right]. \quad (38)$$

Here, we have defined $N \equiv \eta A T_0 P_S / (L + L_S)^2$ as the mean photoelectron count registered per source coherence time, given that the mean photon flux of the source is $P_S \equiv \int d\boldsymbol{\rho} I_S(\boldsymbol{\rho})$, and

$$\Gamma \equiv \left| \frac{K_O^{(n)}(\boldsymbol{\rho}_d; L + L_s)}{K_O^{(n)}(\mathbf{0}; L + L_s)} \right|^2 \in [0, 1], \quad (39)$$

as the equal-time correlation coefficient between the photocurrents registered at the two detectors, given in terms of K_O defined in Eq. (10). We have also assumed here, for convenience, that the photodetectors are identical in specification, i.e., that $\eta_1 = \eta_2 = \eta$ and $A_1 = A_2 = A$.

It is useful to consider two limiting cases of this expression based on whether the incident light is broadband relative to the photodetector ($\Omega_B T_0 \ll 1$), or whether the incident light is narrowband relative to the photodetector ($\Omega_B T_0 \gg 1$). Because naturally-occurring light sources are nominally broadband and are filtered optically at the measurement plane, typically the former limit will hold. However, when pseudothermal light sources are generated in the laboratory it is possible that the latter limit is true. Hence, here we report on both limits.

In the $\Omega_B T_0 \ll 1$ (broadband) limit, the Eq. (32) expression simplifies to

$$\text{SNR}^{(\text{bb})} \approx \cos^2(\theta_d) \alpha T \Omega_B \Gamma \left[\frac{\sqrt{2}}{\sqrt{\pi} N^2} + \frac{2\sqrt{2}}{N} + \sqrt{2\pi}(1 + \Gamma^2) \right]^{-1}. \quad (40)$$

The photodetector currents decorrelate over approximately Ω_B^{-1} intervals, thus the SNR is proportional to the product $T \Omega_B$. For $N \ll 1$, the signature is photon starved and the SNR has a quadratic dependence on mean photon flux. As N increases, the SNR approaches its maximum value

$$\text{SNR}_{\text{max}}^{(\text{bb})} = \cos^2(\theta_d) \alpha T \Omega_B \frac{\Gamma}{\sqrt{2\pi}(1 + \Gamma^2)}. \quad (41)$$

Figure 4(a) plots the transition of the normalized SNR from the photon-starved region to its maximum, as a function of N .

In the $\Omega_B T_0 \gg 1$ (narrowband) limit, on the other hand, the Eq. (32) expression is

$$\text{SNR}^{(\text{nb})} \approx \cos^2(\theta_d) \alpha \Gamma \frac{T}{T_0} \left[\frac{\sqrt{2}(1 + \Gamma)}{\sqrt{\pi} N^2 T_0 \Omega_B} + \frac{(1 + 2\Gamma)}{N} + \frac{\sqrt{\pi}}{2\sqrt{2}} (1 + 2(\sqrt{2} + 1)\Gamma + (1 + 2\sqrt{2})\Gamma^2) \right]^{-1}. \quad (42)$$

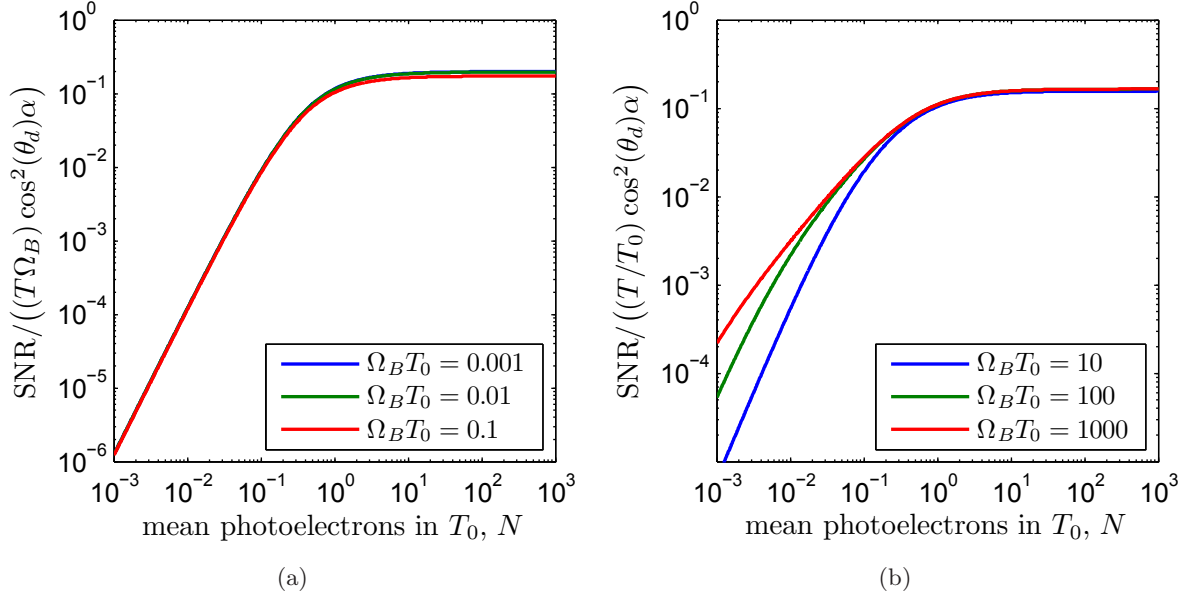


Figure 4. The normalized signal to noise ratio (SNR) of the differential intensity covariance measurement is plotted as a function of N . $\Gamma = 1$ is assumed. (a) When the incident optical field is broadband relative to the detector bandwidth (i.e., $T_0\Omega_B \ll 1$). In this case the normalized SNR has little dependence on the $T_0\Omega_B$ product. (b) When the incident optical field is narrowband relative to the detector bandwidth (i.e., $T_0\Omega_B \gg 1$). In this case the normalized SNR in the $N \ll 1$ regime has a dependence on the $T_0\Omega_B$ product, but the maximum (attained when $N \gg 1$ is independent of this product.

When the source is narrowband relative to the detectors, the photocurrent correlation time is approximately T_0 , so the SNR is now proportional T/T_0 . For $N^2T_0\Omega_B \ll 1$, the signature is photon starved and the SNR has a quadratic dependence on mean photon flux. As N increases, if $N\sqrt{T_0\Omega_B} \gg 1$ and $N \ll 1$ simultaneously hold, then the SNR becomes linear in N . For $N \gg 1$ it saturates to its maximum value,

$$\text{SNR}_{\text{max}}^{(\text{nb})} = \cos^2(\theta_d)\alpha \frac{T}{T_0} \frac{2\sqrt{2}\Gamma}{\sqrt{\pi}(1 + 2(\sqrt{2} + 1)\Gamma + (1 + 2\sqrt{2})\Gamma^2)}. \quad (43)$$

Figure 4(b) illustrates the variation of the normalized SNR as a function of N in the narrowband case.

5. CONCLUSIONS

Motivated by the recent resurgence of interest in intensity interferometry, in this paper we have analyzed the perturbative intensity-correlation signature due to small objects passing between a known source and the measurement detectors. In particular, we have derived an analytic approximation to the intensity covariance of an extended source partially-occluded by an absorptive object, such as a planet. We have applied the results to both a parameter set that could represent a table-top demonstration, and a parameter set that would be applicable to a stellar imaging scenario. We showed that a differential measurement—which subtracts the baseline covariance of the source alone from the covariance measured with the object present—yields a fluctuation that arises from the presence of the object. We then derived this interferometric signature explicitly assuming disc-shaped objects. Finally, we evaluated tractable analytic expressions for the SNR, showing that at low signal flux values the SNR has a quadratic scaling with incident photon number (per coherence duration of the source), but that as this quantity increases the scaling saturates to a constant.

There are several conclusions to draw from our analysis. First, returning to Eq. (18), we conclude that the intensity covariance measurement is the magnitude-square of the difference between the spatial Fourier transforms of the source and the absorptive object. Thus, using reasonable assumptions on the nonzero domain of this expression's inverse Fourier transform, it is feasible that iterative phase-retrieval algorithms, such as

the Gerchberg-Saxton algorithm, can reconstruct images of arbitrary objects that are partially occluding the source.^{11,12} Phase-retrieval techniques have found wide application in optical imaging, including in intensity interferometry. A second conclusion that can be drawn from our exposition in Section 3 is that the intensity covariance has an imprint of the displacement of the object relative to the axis along which the measurements are being performed. Thus, if several consecutive snapshots of the intensity correlation are obtained it is feasible to estimate the axis of motion for a (dynamic) object, such as a planet orbiting a distant star.

Historically stellar intensity interferometry has been challenged by its low SNR. Our derivations of the SNR are consistent with this conclusion. Due to our assumption that the object of interest is small relative to the source, the mean signature (i.e., the intensity covariance perturbation due to the object) is proportional to γ^2 , where γ is the ratio of the object's diameter to that of the source. Consequently, we find that the SNR of this measurement scales with γ^4 . Furthermore, because the intensity correlation measurement relies on common-mode fluctuations of photocurrents from the two detectors, it is often photon starved. For example, consider the parameter set in Table 1 corresponding to imaging an Earth-size planet orbiting our sun, from a distance commensurate with Kepler 20f. Assuming, for convenience, that we are imaging at $1\ \mu\text{m}$ center wavelength with $1\ \text{nm}$ optical bandwidth, that we have a photodetector with $\Omega_B/2\pi = 10\ \text{GHz}$ electrical bandwidth and quantum efficiency 0.9, and that we have large-aperture telescopes with $A = 4.5\ \text{m}^2$, we find that $N \approx 1.5 \times 10^{-8}$. Thus, the SNR is well into the regime in which it is proportional to N^2 , so, even with a generous 10-hour integration time the SNR is impractically low. Nonetheless, shortening the distance between the source and the measurement planes improves the SNR by the fourth power (until $N \approx 1$), so a reduction by a factor of 100 would be sufficient to approach the maximum SNR scaling found in Eq. (41). Consequently, while our analysis predicts somewhat negative results for stellar imaging at distances comparable to those in current missions, it does imply that intensity interferometry would be feasible at moderate distances. On the other hand, the parameter set we have used for a laboratory experiment has more forgiving results. Here, we find that $N \approx 550$ with a $1\ \text{mW}$ pseudothermal source having $T_0 \approx 0.02\ \text{ms}$, a $10\ \text{MHz}$ photodetector having quantum efficiency 0.7, and two $100\ \mu\text{m}$ -diameter pinhole apertures for the detectors. This predicts $\text{SNR} \approx 1.5$ with $T = 2\ \text{s}$.

In summary, we have analyzed the perturbations in the intensity covariance signature of a source when a small object partially occludes it. We have derived the mean signature as well as the SNR of this measurement, showing that the Fourier transformation of its absorptivity can be determined provided that the source intensity covariance and the propagation medium are known. When the SNR results are applied to stellar imaging applications of current interest, we have found that it is likely too low due to the paucity of common-mode photons at the two detectors. However, we have shown that for shorter distances intensity interferometry may facilitate the estimation of some object features that would otherwise not be discernable from the fluctuations in the observed brightness.

ACKNOWLEDGMENTS

This research was supported by the NASA Innovative Advanced Concepts (NIAC) program, and was carried out by the Jet Propulsion Laboratory, California Institute of Technology, under a contract with the National Aeronautics and Space Administration. BIE is currently at Google Inc., but his contributions to this work were carried out at Jet Propulsion Laboratory.

REFERENCES

1. R. Hanbury Brown and R. Q. Twiss, "A test of a new type of stellar interferometer on Sirius," *Nature* **178**, pp. 1046–1048, 1956.
2. I. Klein, M. Guelman, and S. G. Lipson, "Space-based intensity interferometer," *Appl. Opt.* **46**, p. 4237, 2007.
3. D. Dravins and S. LeBohec, "Toward a diffraction-limited square-kilometer optical telescope: Digital revival of intensity interferometry," *Proc. SPIE* **6986**, p. 698609, 2008.
4. R. B. Holmes, S. Lebohec, and P. D. Nunez, "Two-dimensional image recovery in intensity interferometry using the cauchy-riemann relations," *Proc. SPIE* **7818**, p. 78180O, 2010.

5. S. LeBoheca, B. Adamsa, I. Bondb, S. Bradburyb, D. Dravinsc, H. Jensenc, D. B. Kiedaa, D. Kressa, E. Munforda, P. D. N. neza, R. Pricea, E. Ribakd, J. Roseb, H. Simpsona, and J. Smitha, “Stellar intensity interferometry: Experimental steps toward long-baseline observations,” *Proc. SPIE* **7734**, p. 77341D, 2010.
6. R. Holmes, B. Calef, D. Gerwe, and P. Crabtree, “Cramer-Rao bounds for intensity interferometry measurements,” *Appl. Opt.* **52**, pp. 5235–5246, 2013.
7. B. I. Erkmen and J. H. Shapiro, “Ghost imaging: from quantum to classical to computational,” *Adv. Opt. Photon.* **2**, pp. 404–450, 2010.
8. L. Mandel and E. Wolf, *Optical Coherence and Quantum Optics*, Cambridge Univ., Cambridge, 1995.
9. J. W. Goodman, *Statistical Optics*, Wiley, New York, Classics ed., 2000.
10. F. Fressin, G. Torres, J. F. Rowe, D. Charbonneau, L. A. Rogers, S. Ballard, N. M. Batalha, W. J. Borucki, S. T. Bryson, L. A. Buchhave, D. R. Ciardi, J.-M. Désert, C. D. Dressing, D. C. Fabrycky, E. B. Ford, T. N. Gautier III, C. E. Henze, M. J. Holman, A. Howard, S. B. Howell, J. M. Jenkins, D. G. Koch, D. W. Latham, J. J. Lissauer, G. W. Marcy, S. N. Quinn, D. Ragozzine, D. D. Sasselov, S. Seager, T. Barclay, F. Mullally, S. E. Seader, M. Still, J. D. Twicken, S. E. Thompson, and K. Uddin, “Two Earth-sized planets orbiting Kepler-20,” *Nature* **482**, pp. 195–198, 2011.
11. J. R. Fienup, “Phase retrieval algorithms: a comparison,” *Appl. Opt.* **21**, pp. 2758–2769, 1982.
12. J. R. Fienup, “Phase retrieval algorithms: a personal tour [Invited],” *Appl. Opt.* **52**, pp. 45–56, 2013.